Construction and Building Materials 198 (2019) 512–526

Contents lists available at ScienceDirect

Construction and Building Materials

journal homepage: www.elsevier.com/locate/conbuildmat

Thermal and mechanical properties of structural lightweight concrete containing lightweight aggregates and fly-ash cenospheres

Hongyu Zhou *, Adam L. Brooks

Civil and Environmental Engineering, University of Alabama in Huntsville, Huntsville, AL 35899, USA

HIGHLIGHTS

- Mechanical and thermal properties of lightweight concrete containing lightweight aggregates and fly ash cenospheres (FAC) are studied.
- Microstructural investigation is performed to reveal the interaction mechanisms between fillers, aggregates, and the cement matrix.
- Analytical approach was proposed to calculate the thermal property of lightweight concrete with various types of aggregates and FAC.

ARTICLE INFO

Article history:
Received 13 February 2018
Received in revised form 25 October 2018
Accepted 9 November 2018

Keywords:
Lightweight concrete
Mechanical and thermal behaviors
Fly-ash cenospheres
Thermal modeling

ABSTRACT

This study investigates the effects of mix proportion, aggregate type, and microstructures on the thermal and mechanical behaviors of structural lightweight concrete (LWC) containing lightweight aggregates and lightweight functional fillers such as fly-ash cenospheres (FAC). Particularly, FAC are incorporated into the mixtures to reduce the materials' density and thermal conductivity while maintaining high mechanical strength. The experimental results indicate that the elastic modulus and thermal conductivity of LWC decrease linearly with respect to the reduction in concrete density, while compressive strength depend largely on material microstructures. The hierarchically porous microstructure of FAC-containing LWC were investigated using scanning electron microscopy (SEM) and the interactions between lightweight fillers and other phases in concrete – i.e., the cementitious binder and aggregates – are investigated. SEM images taken on mechanically tested LWC samples indicated that the strong FAC shell may provided barriers to hinder micro-crack formation and propagation. Lastly, a two-step homogenization scheme was proposed to estimate the thermal properties of lightweight concrete containing both FAC and aggregates. The results calculated using this method shows good agreement with experimental data.

1. Introduction

Due to its advantageous properties including low density, good thermal insulation and fire resistance, lightweight concrete (LWC) has been widely studied both as structural and nonstructural building material [1]. Traditionally, structural lightweight concrete are produced by incorporating coarse lightweight aggregates (LWA) such as pumice, perlite [2–4], expanded shale [5–7] and expanded clay [1] into the mixture. Many applications of lightweight aggregate concrete (LWAC) can be found in structures such as long span bridges, high rise buildings, and special structures such as floating and offshore platforms [8]. For LWC that are used for structural load bearing purposes, minimum design strengths are often prescribed for specific applications [9]. The density of structural LWAC normally varies between 1500 and 2000 kg/m^3 depending on the type and volume fraction of LWA used. While the unit weight of conventional LWAC materials has been successfully achieved within the stipulated guidelines [10,11], traditional LWAC has shown lower mechanical strength and reduced performance such as impaired durability [1] and brittle failure [12]. In addition, for building applications where high insulation is desired, portions of the fine normal weight aggregate (NWA) within LWC are also replaced by LWA to further reduce thermal conductivity of the concrete [13]. The further decrease in density leads to inferior mechanical strength (often < 15 MPa), rendering the materials not suitable for structural use [8].

To circumvent some drawbacks of conventional LWAC, a type of high strength (ultra-)lightweight cementitious composite materials were developed by incorporating micrometer-size fly-ash cenospheres (or FACs) into cement based matrix to form a microcellular cementitious composite (Zhou et al. [14], Wu et al. [15],

* Corresponding author at: 5000 Tech. Drive, Huntsville, AL, USA.
E-mail address: hongyu.zhou@uah.edu (H. Zhou).

https://doi.org/10.1016/j.conbuildmat.2018.11.074
0950-0618/

Xu et al. [16], and Liu et al. [17]). Fly-ash cenosphere, which is an alumino-silicate based by-product of coal combustion at thermal power plants [18], are particles that have a spherical shape and hollow interior covered by a thin shell with typical shell thickness of about 5–15% of its diameter. Because of its hollow structure, FAC have low particle density and low thermal conductivity. In addition, most FAC have partial pozzolanic reactivity, which helps to develop interfacial bonding with cementitious binders. Because of these properties, FAC have been used for the development of high strength, low density cementitious composite materials with low thermal conductivity (below 0.4 W/m K) and high specific strength (0.047 MPa/kg/m^3) [15,19].

Despite the studies conducted separately for LWAC and cementitious composites containing FAC (e.g., ULCC), there still lacks an understanding of the synergy between the micro-size fillers and other material phases in concrete (e.g., fine and coarse aggregates). In addition, existing research on lightweight concrete shows a significant variation regarding both mechanical and thermal properties affected by constituent materials and mix proportions [20]. Most studies to date on LWC focused either only on obtaining a material suitable for structural load-bearing purposes with high strength or as nonstructural material with low thermal conductivity. Few studies have been conducted to address the balance between mechanical properties and thermal properties [15,19–21]. To that end, understanding the effects of mix proportion, aggregate property, and microstructures on material macroscopic properties becomes crucial. In this research, a comprehensive study is conducted on concrete and cementitious composites that contain various types of aggregates (i.e., both natural and lightweight coarse and fine aggregates) as well as lightweight functional fillers such as FAC. The material thermophysical (i.e., density, thermal conductivity, and specific heat capacity) and mechanical (elastic modulus and compressive strength) properties are investigated with respect to the mix proportion, aggregate type, and properties of the binder material (i.e., water to cementitious material ratio (W/C), fiber reinforcements). Key parameters governing the material thermal and mechanical properties are discussed, and a two-stage homogenization model is proposed for the prediction of the materials' thermophysical properties. The materials developed by this approach will have a good balance between the mechanical and thermal properties which can be used towards monolithic green building design.

2. Experimental program

2.1. Mixture design and material preparation

In this study, three series of normal and lightweight concrete mixtures were prepared with three binder types – i.e., normal strength (NS) cement matrix, high strength (HS) matrix with 15% cement replaced by silica fume, and HS matrix reinforced with steel fiber (SF) (20 wt% of cement, 1.49% by volume). Within each series, different aggregate types were tested with a combination of coarse and fine normal weight aggregates (NWA) and LWA. Normal weight concrete (NWC) mixtures having only NWA were tested as control groups. The LWC were designed with different size LWA to (partially) replace coarse and fine NWA. FAC was also tested as a lightweight filler to partially replace fine NWA (~50% by volume). The mix proportions of the 14 concrete mixtures tested are listed in Table 1, and the dry density tested in this study ranges from 1421 kg/m^3 to 2488 kg/m^3.

The binder material used for preparing the concrete consists of ASTM Type I-II Portland cement and silica fume, see Fig. 1. The water to cementitious material ratio was selected at 0.35 for normal strength mixtures and 0.27 for high strength mixtures. A polycarboxylic ether-based superplasticizer (*Sika*) was used to adjust the workability. The lightweight aggregates (both coarse and fine) used here are commercially available products manufactured from expanded clay in the Southeast of the US (*Trinity Lightweight*). These LWA contain a number of close-cell air pores (cellular structure), as can be seen in Fig. 2. The porosity and pore-size distribution within the LWA were measured using mercury intrusion porosimetry (MIP). The LWA have moderate specific densities (~830 kg/m^3) and relatively high mechanical strength, which make them suitable for producing structural lightweight concrete. Ground quartz flour, with the density of 2650 kg/m^3, was used as filler to adjust the powder amount and reduce the air content within the mortar. Fly-ash cenospheres (FAC), with average particle size of 81 μm and particle density of 910 kg/m^3 were used as lightweight functional filler to partially replace fine NWA and induce micrometer-size air cell in the cementitious matrix. Steel fiber (*Nycon*), with 0.2 mm diameter and 13 mm length was investigated as reinforcements for the high strength LWC.

The particle size, gradation, and other physical properties of aggregates are shown in Fig. 3 and Table 2. X-ray diffraction (XRD) analysis performed on the RiverLite™ LWA indicates that

Table 1
Test matrix and mix proportions (by weight, kg of materials/m^3 of concrete).

Mix ID*	Binder		Water	W/(C + F)	FAC	Quartz Flour	Steel Fiber	Silica Sand	Gravel (Lime Stone)	Lightweight Aggregate	
	Cement	Silica Fume								RiverLite™ (Fine)	RiverLite™ (Coarse)
NS-SS-G	437.4	–	153.2	0.35	0.0	–	–	734.7	874.7	–	–
NS-FAC/SS-G	437.4	–	153.2		96.0	–	–	410.2	874.7	–	–
NS-FAC/RLF-G	437.4	–	153.2		96.0	–	–	0.0	874.7	216.5	–
NS-SS-RLC	437.4	–	153.2		0.0	–	–	734.7	0.0	–	377.0
NS-FAC/SS-RLC	437.4	–	153.2		96.0	–	–	410.2	0.0	–	377.0
NS-FAC/RLF-RLC	437.4	–	153.2		96.0	–	–	0.0	0.0	216.5	377.0
HS-SS-G	489	86.3	155.3	0.27	–	253.3	–	431.2	816.7	–	–
HS-FAC/SS-G	489	86.3	155.3		107.3	141.5	–	234.3	816.7	–	–
HS-SS-RLC	489	86.3	155.3		–	253.3	–	431.2	–	–	355.8
HS-FAC/SS-RLC	489	86.3	155.3		107.3	141.5	–	234.3	–	–	355.8
HS-SS-G-SF	481.5	85.0	153.0	0.27	–	249.4	116.1	424.7	804.4	–	–
HS-FAC/SS-G-SF	481.5	85.0	153.0		105.7	139.4	116.1	230.7	804.4	–	–
HS-SS-RLC-SF	481.5	85.0	153.0		–	249.4	116.1	424.7	–	–	350.4
HS-FAC/SS-RLC-SF	481.5	85.0	153.0		105.7	139.4	116.1	230.7	–	–	350.4

SS – Silica Sand; G – Natural limestone gravel; RLC – RiverLite™ Coarse LWA; RLF – RiverLite™ Fine LWA; -SF – Steel fiber reinforced;
FAC/SS – 50% of fine NWA are replaced by FAC; FAC/RLF – fine aggregates are only comprised of FAC and RLF.
* NS- – Normal strength cement binder; HS- – High strength cement binder with silica fume and lower water to binder ratio.

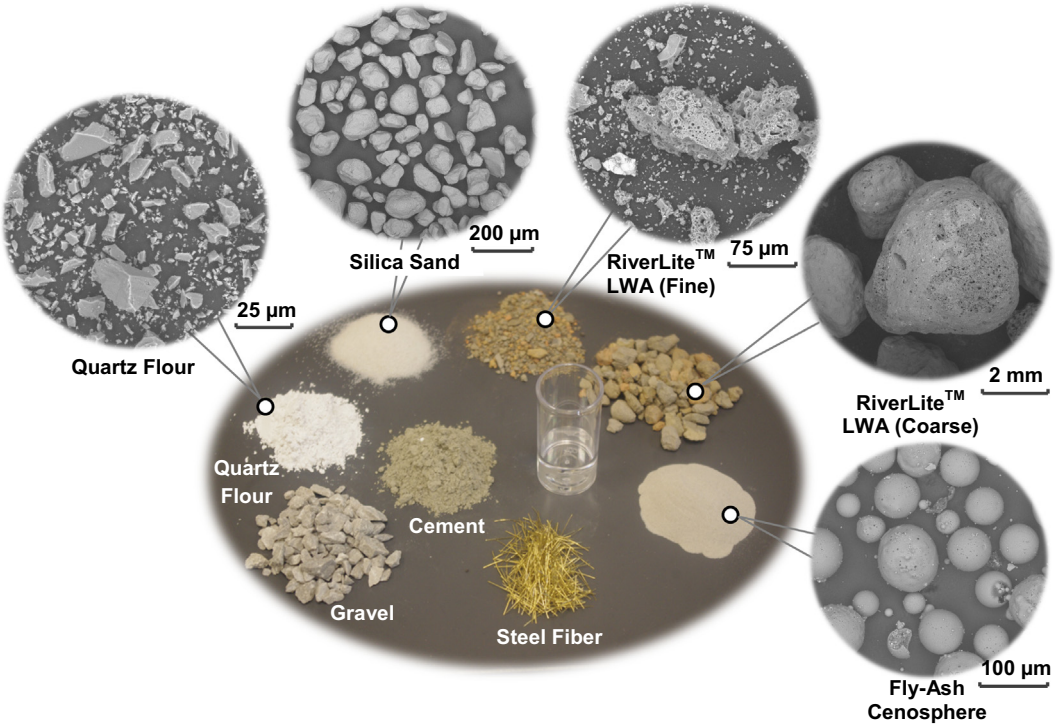

Fig. 1. Common ingredients within structural lightweight concrete.

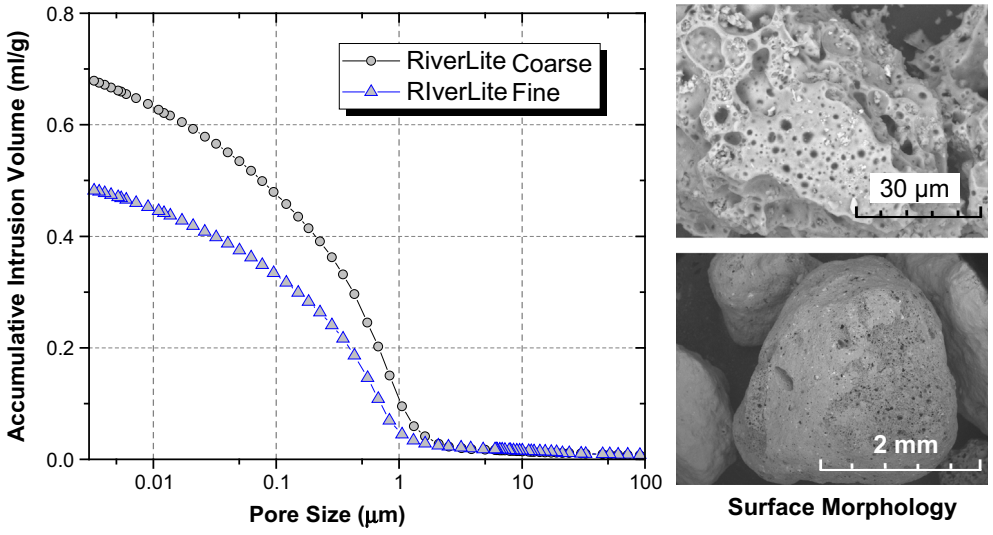

Fig. 2. The mercury intrusion porosimetry (MIP) test and SEM imaging performed on RiverLite™ LWA.

the material is primarily comprised of amorphous materials and crystalline minerals including quartz, spinel, and millosevichite, see Fig. 3(a). Since water absorption of LWA is an influential factor in the lightweight aggregates concrete design and production – i.e., if mixed in dry condition the LWAs normally absorb a certain amount of free water from the fresh mixture. Therefore, the LWAs were immersed in water for 24 h until reaching saturation. The aggregates were then drained on a US #30 standard sieve with periodic mechanical agitation (shaking) for 3–4 h until they reach surface dry (SD) condition before mixing – i.e., the SD conditions for both coarse and screened-fine LWA were determined according to ASTM C127-15 and ASTM C128-15 specifications, respectively. The specific densities of LWA were also measured under SD condition for the mix proportion design, see Table 2. The cenospheres used in this research have particle sizes up to 106 µm (*E106, CenoStar*). XRD analysis performed on the FAC (Fig. 3(a)) indicated that the cenospheres are comprised primarily of amorphous materials with small amounts of mullite and calcite. The particle size distribution of cenosphere particles was analyzed using a laser diffraction particle size analyzer (*Horiba LA-950*) and the results are plotted in Fig. 3(b).

2.2. Methods for mechanical and thermal testing

2.2.1. Experimental setup for mechanical tests

The mechanical tests were performed using a 500 kN MTS-810 servo-hydraulic universal testing system as shown in Fig. 4(a). Five 101.6 mm (4 in.) diameter by 203.2 mm (8 in.) cylinders were

tested for each specimen group listed in Table 1. The mechanical loading procedure was carried out in a displacement-control mode at the loading rate of 0.01 mm/min. The deformation (i.e., compressive strain) of test cylinders was measured using a pair of clamp-on extensometers (*Epsilon Tech*) with gauge length of 50 mm. The extensometer pair was clamped onto the specimen to measure the strains on both sides of the cylinder. The setup of extensometers is shown in Fig. 4(b). A high resolution CCD camera was staged to record the damage and failure of the specimens. The tested specimens were preserved for scanning electron microscopy (SEM) analysis.

2.2.2. Thermal property measurement using transient plane source (TPS) method

The transient plane source (TPS) method originally developed by Gustafsson [22] was applied to measure the thermal properties of the aggregates (see Table 2) and concrete. The TPS technique is based on the recorded temperature rise of a plane source that heats the surrounding material to be measured. In a TPS test, a conducting pattern with negligible heat capacity (e.g., Kapton supported double spiraled nickel metal sensor as shown in Fig. 5(a)) serves simultaneously as the heat source and the temperature sensor. The initial electrical resistance of the TPS element, R_0, is first balanced in a Wheatstone bridge and, during the measurements, the unbalanced voltage drop $\Delta V(t)$ is recorded as the function of time t using a high-impedance digital voltmeter, where $\Delta V(t)$ has the following expression [22]:

$$\Delta V(t) = \frac{R_s R_0^2}{R_0 + R_s} \frac{I_0^3 \alpha}{\pi^{2/3} a} \frac{D(\tau)}{k} \tag{1}$$

where R_s is the standard resistance in the Wheatstone bridge circuit, I_0 is the heating current, α is the temperature coefficient of the TPS element, a is the outer radius of the heating element, k is the thermal conductivity of the material, and $D(\tau)$ is a function that can be tabulated for a particular TPS element as a function of the dimensionless parameter $\tau = (\kappa t/a^2)^{1/2}$, where κ is the thermal diffusivity of the material to be tested. Through a process of iteration, the thermal conductivity k and thermal diffusivity κ of the tested material can be simultaneously obtained from one single transient recording [23].

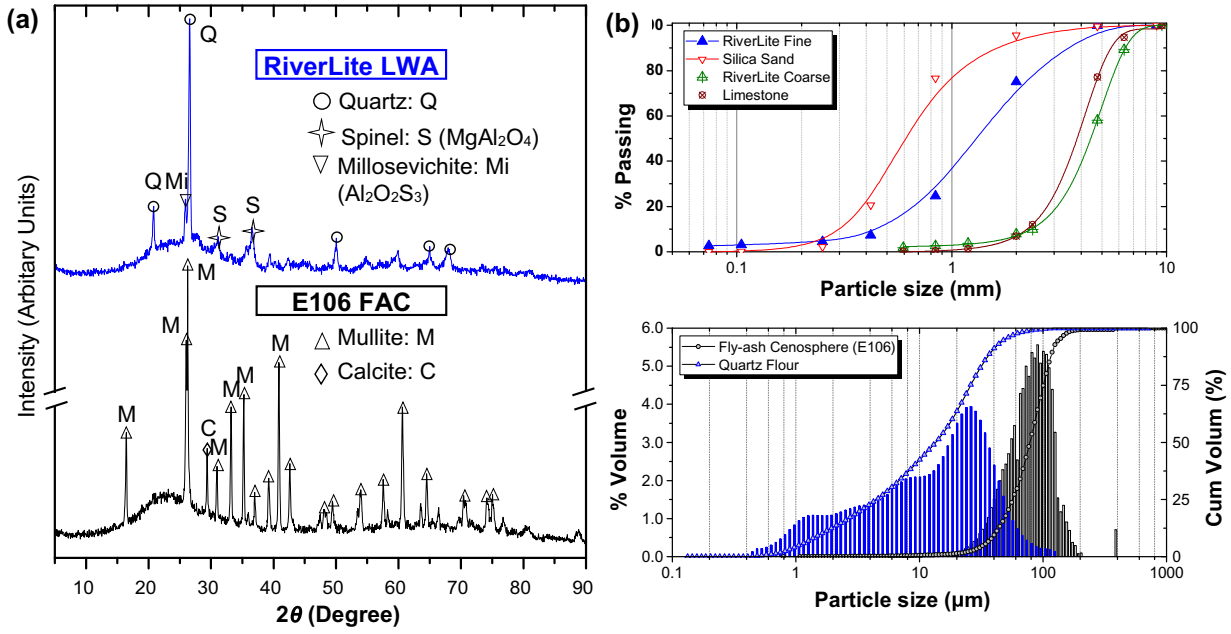

Fig. 3. Characterization test performed on aggregates: (a) XRD spectrum for LWA and FAC; and (b) particle size analysis results and gradation.

Table 2
Aggregate properties.

	Particle Size*			Bulk Density**	Specific Density	Porosity***	Thermal Conductivity****
	D_{10}	D_{50}	D_{90}				
		um		kg/m³	kg/m³	Vol %	W/mK
Silica Sand	300	600	1350	1497 (1673)	2650	–	4.0
Quartz Flour	1.60	13.6	38.6	867 (1066)	2650	–	5.5
Fly-ash Cenosphere (E106)	42.6	81.3	125.2	394 (4 4 2)	910	–	–
Steel Fiber	–	–	–	–	7850	–	54
Limestone	2150	3800	6200	1414 (1551)	2570 (2610)*	–	3.03
RiverLite™ LWA (coarse)	2200	4300	5300	514 (5 5 6)	830 (1150)*	57.9	0.190
RiverLite™ LWA (Fine)	440	1250	3400	709 (7 8 7)	830 (1150)*	49.15	0.190

* The specific density of coarse aggregates is reported in both oven-dry and saturated surface dry conditions according to ASTM C127 and C128 specifications.
** Bulk density is reported both in loosely packed and (vibrated) states.
*** The porosity of LWA is tested using mercury intrusion porosimetry (MIP).
**** Thermal conductivities of aggregates were tested using transient plane source method (ISO22007), also see Fig. 5(c).

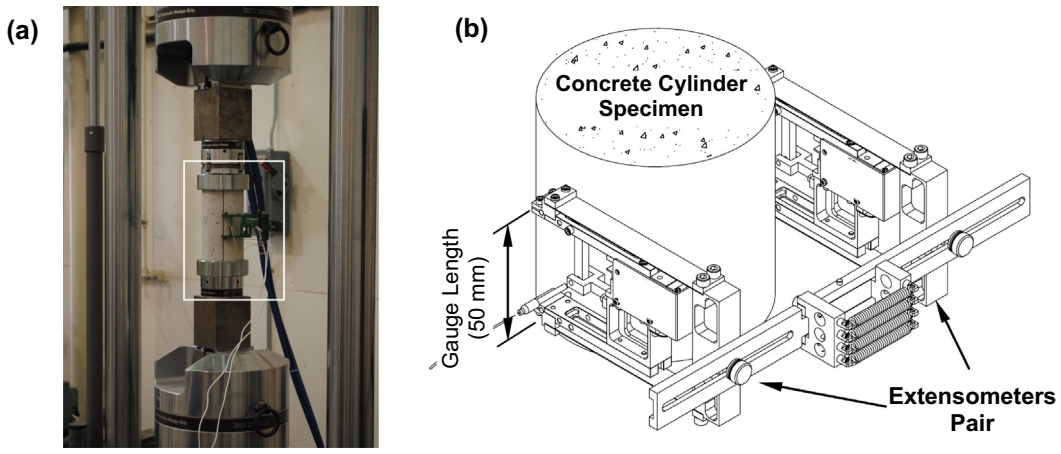

Fig. 4. Mechanical test setup: (a) picture showing the compressive cylinder used to determine mechanical properties; and (b) setup of extensometers for Young's modulus measurement.

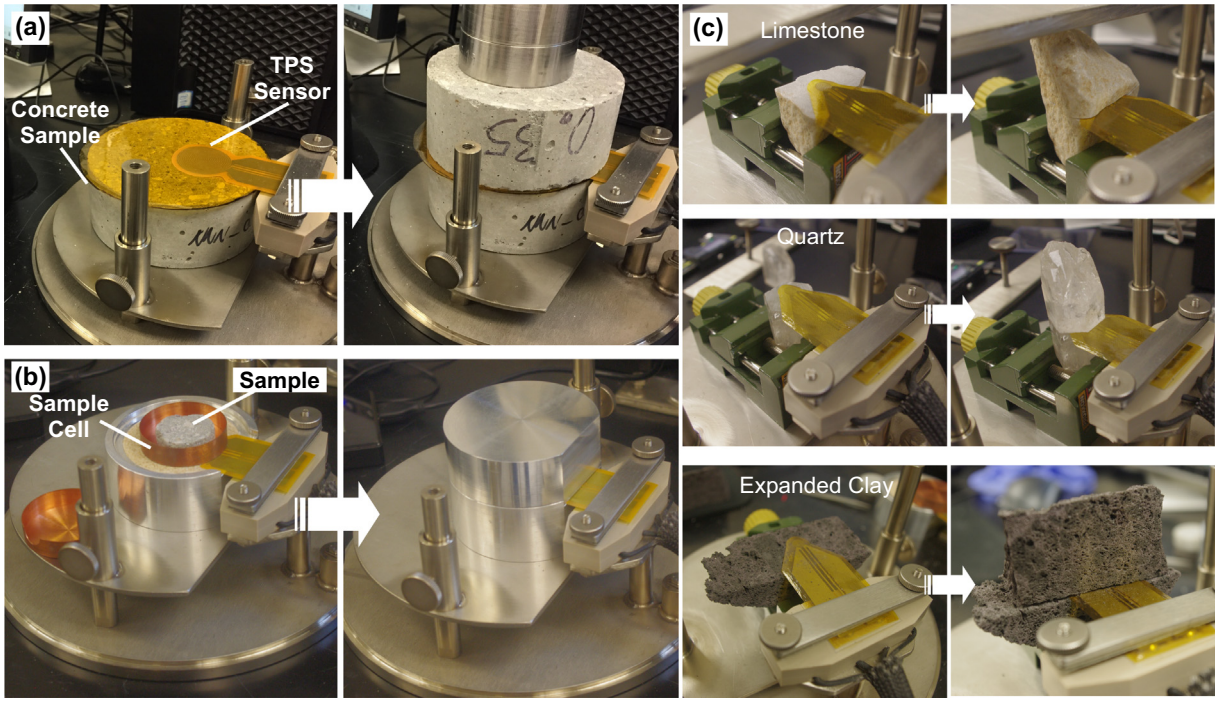

Fig. 5. The Transient Plane Source (TPS) method for thermal constants analysis: (a) TPS measurement on concrete samples; (b) specific heat capacity measurement; and (c) TPS test setup for aggregates: gravel (limestone), silica sand (quartz), and LWA (sintered expended clay).

While the specific heat capacity of the tested materials can be deduced from the thermal conductivity k and the thermal diffusivity κ as outlined by Eq. (1) using a single set of TPS data, a more reliable method for measuring materials' specific heat capacity was developed [24]. In a specific heat measurement, a TPS sensor is attached to the underside of a conductive sample holder made of gold or copper and disc shape samples with 25 mm diameter and 10 mm height is used for the specific heat measurement. The process of measuring is based on two individual measurements; a reference measurement (the empty container) and a sample measurement (the container while holding a sample). In order to minimize the heat losses to ambient air, the setup of the sensor, sample holder and the sample to be measured are all encased in a thermal insulating chamber, see Fig. 5(b). The method is based on the assumption of a linear temperature increase – i.e., the heat losses to the surroundings are assumed negligible for the time span of the measurement. The heat capacity would be calculated by Eq. (1) as for the adiabatic calorimetry [24]:

$$mc_p = \frac{\Delta E}{\Delta T} = \frac{\int_{t_2}^{t_2} V(t) I_0 dt}{\Delta T} \tag{2}$$

where m is the sample mass, c_p is the specific heat capacity, and ΔT is the temperature change. It is noted that to find the right time span for the analysis, the measurement data could be analyzed in a variety of time windows. The results will give a curve with a maximum that is close to the specific heat of the analyzed material [24].

For thermal conductivity measurements, three pairs of disc shaped concrete samples (100 mm diameter and 25 mm thick) were prepared. The TPS tests were performed using a *HotDisk TPS-1500* thermal constant analyzer with a 29.22 mm diameter TPS sensor according to the ISO22007-2 specifications [25]. The sensor size is

in accordance with the guidelines set out for heterogeneous samples with grain size up to 10 mm. The applicable thermal conductivity testing range of the equipment was 0.01–400 W/m K. In addition, 25 mm diameter 9 mm tall disc shape concrete samples were machined for specific heat capacity measurements. The sample size is comparable with the maximum aggregate size used in the concrete. All samples were dried in a convection oven for 48 h and cooled down to room temperature in an air-tight desiccant cabinet to prevent surface condensation. The thermal conductivity of aggregates – i.e., silica sand (quartz), gravel (limestone), and sintered expanded clay (lightweight RiverLite™ coarse and screened fine) were tested from their corresponding parent materials provided by the material producer using the TPS setup, see Fig. 5(c).

3. Results and discussion

3.1. Mechanical and thermophysical properties

3.1.1. Mechanical properties

The densities, mechanical and thermal test results for the concrete mixtures tested are summarized in Table 3. The influence of LWA replacement on concrete mechanical behaviors can be estimated by the relations of concrete mechanical properties to its density. Fig. 6 plots the concrete compressive strength and Young's modulus against the materials' oven dry density. The density is presented in descending order so that the influence of the density decreasing on mechanical properties is displayed. In general, the compressive strength and Young's modulus decrease with concrete density. While at the same density, the concrete might have different compressive strength depending on the strength and type of binder materials used. For similar density, the LWC with steel fiber reinforced high strength binder (HS-xxx-xxx-SF) shows the highest compressive strength. The higher strength matrix provides higher rigidity and strength while steel fiber reinforcements greatly enhance the materials' ability to resist mechanical damage [26]. Nevertheless, the decrease of compressive strength with respect to density is at a substantially higher rate (−9.72 MPa per 100 kg/m^3 decrease in density) for the HS-xxx-xxx-SF group, when replacing the NWA with LWA, than that of the group with normal strength binders (NS-xxx-xxx) (−2.49 MPa per 100 kg/m^3 decrease in density), see Fig. 6(a). This is attributed to the more brittle nature of the higher strength matrix – i.e., the introduction of a weak

Table 3
Experimental results.*

Mix ID	Wet density** kg/m^3	Oven-dry density kg/m^3	Young's modulus GPa	Compressive strength MPa	Thermal conductivity k W/mK	Thermal diffusivity κ mm^2/s	Volumetric Heat capacity (by TPS)*** kJ/m^3	Volumetric heat Capacity (direct measure) kJ/m^3
NS-SS-G	2311	2185	27.07	59.69	1.817	0.954	1904	1902
NS-FAC/SS-G	2177	2039	25.77	46.77	1.386	0.920	1729	1875
NS-FAC/RLF-G	2038	1880	19.38	51.07	1.026	0.674	1522	1806
NS-SS-RLC	1801	1614	15.28	39.11	1.050	0.717	1464	1529
NS-FAC/SS-RLC	1666	1507	12.57	39.10	0.739	0.485	1523	1360
NS-FAC/RLF-RLC	1421	1224	8.84	33.39	0.423	0.334	1267	1130
HS-SS-G	2419	2259	19.93	66.55	1.923	0.964	1995	2031
HS-FAC/SS-G	2204	2063	20.93	60.67	1.437	0.752	1911	1941
HS-SS-RLC	1916	1770	16.50	56.66	1.074	0.709	1514	1585
HS-FAC/SS-RLC	1673	1519	13.18	43.86	0.706	0.473	1492	1412
HS-SS-G-SF	2488	2387	30.83	127.53	2.105	0.972	2165	2370
HS-FAC/SS-G-SF	2360	2228	28.87	100.09	1.607	0.759	2118	1921
HS-SS-RLC-SF	1995	1827	17.51	60.10	1.348	0.786	1714	1603
HS-FAC/SS-RLC-SF	1770	1634	14.36	54.28	0.885	0.564	1570	1447

* Results are presented as the statistical average of measurements on five specimens. The stand deviations are shown as error bars in Figs. 6 and 7.
** Wet density was measured immediately after when concrete was poured.
*** The volumetric heat capacity deducted from the thermal conductivity and thermal diffusivity obtained from a TPS measurement through equation $c_v = k/\kappa$.

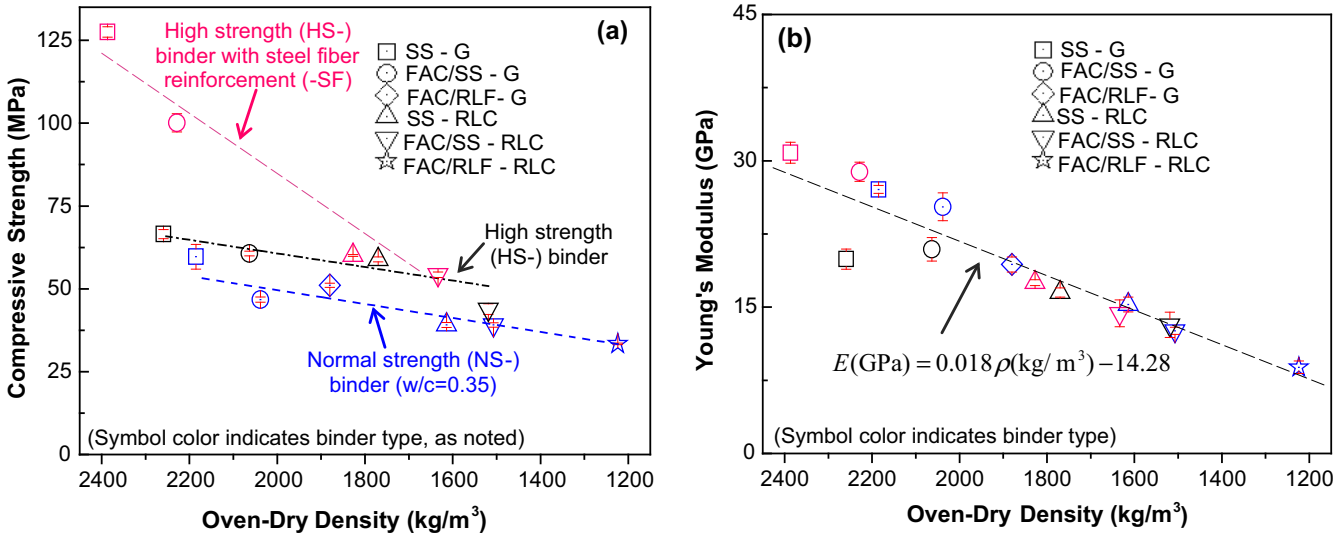

Fig. 6. Relationship between (a) compressive strength and (b) Young's modulus and concrete oven-dry density (error bars indicate the standard deviations of the test results).

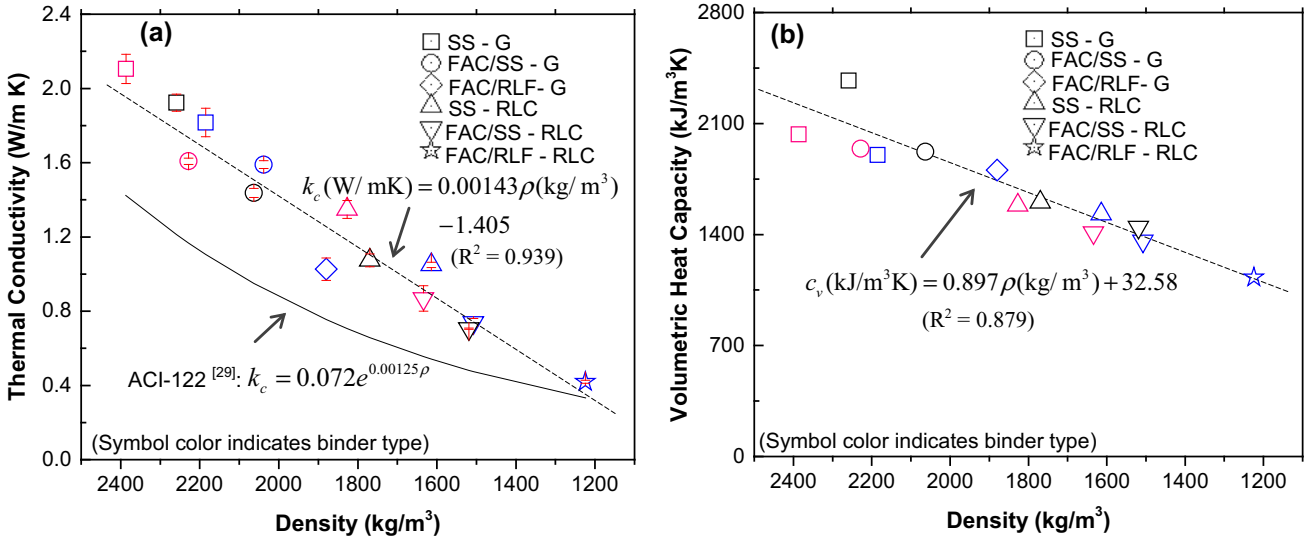

Fig. 7. Thermal properties of LWCC tested through Transient Plane Source (TPS) method: (a) thermal conductivity; and (b) Volumetric heat capacity.

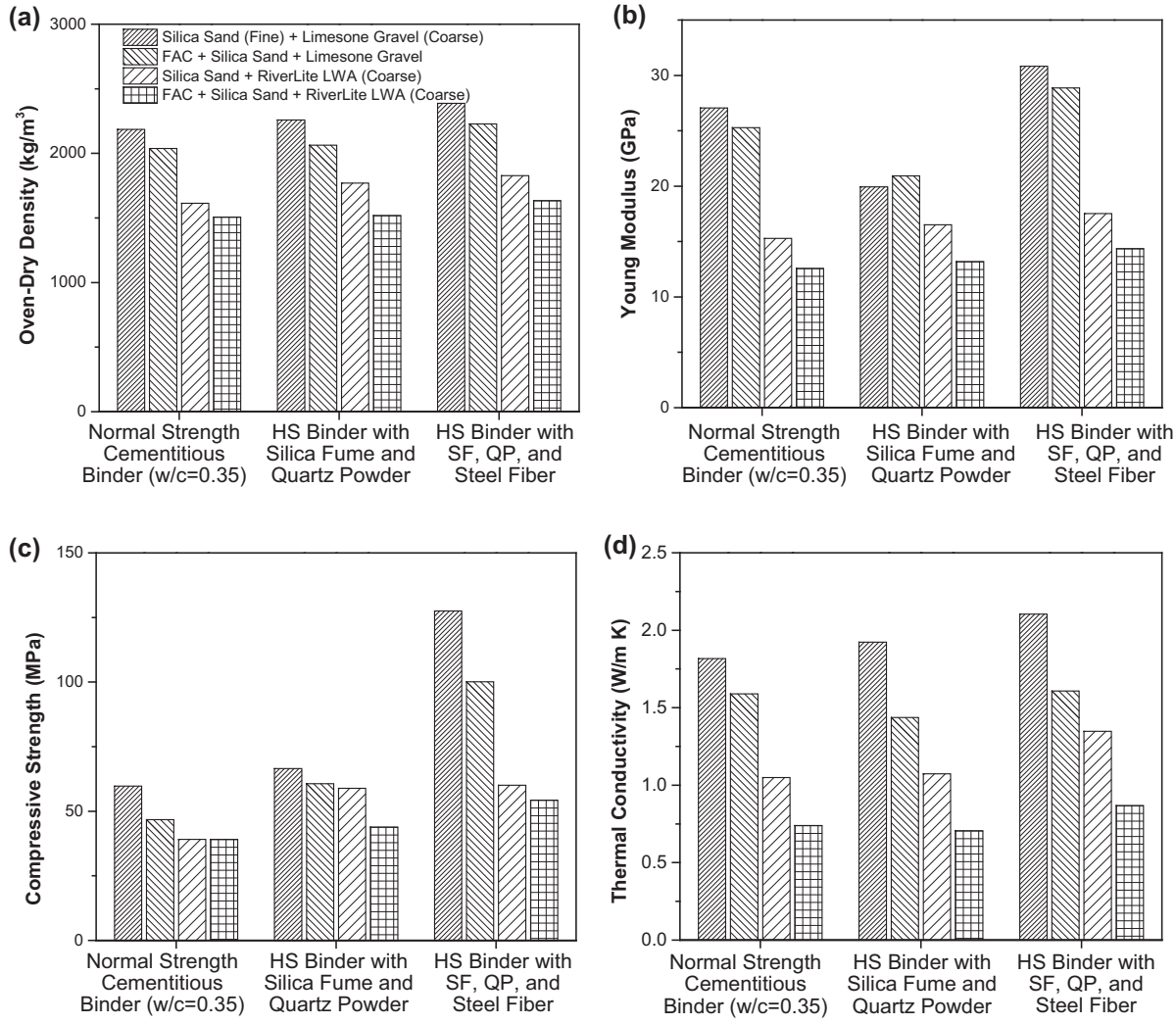

Fig. 8. Effect of aggregates and binder materials on (a) oven-dry density; (b) Young's modulus; (c) compressive strength; and (d) thermal conductivity.

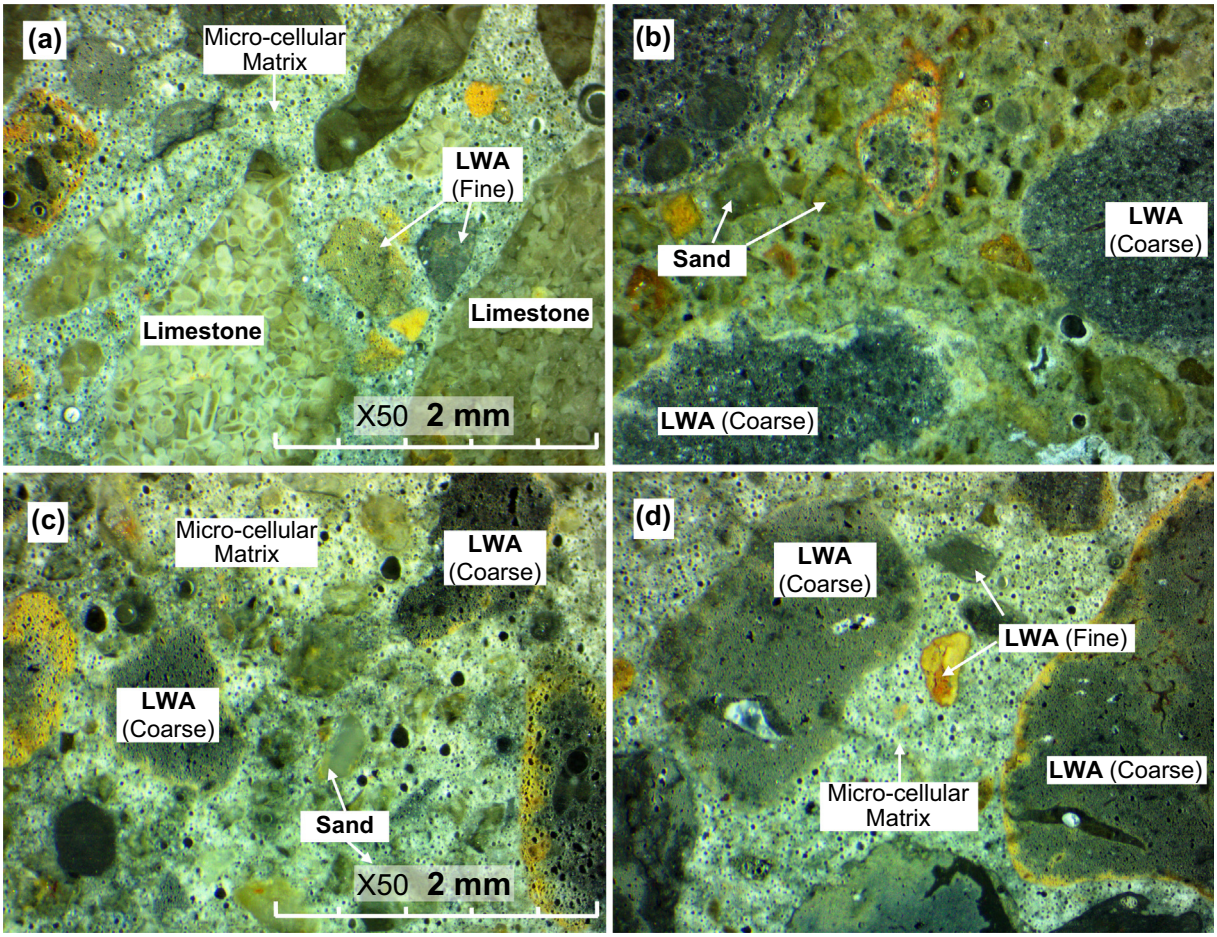

Fig. 9. Optical microscopic images of (a) NS-FAC/RLF-G (Fine NWA replaced by FAC and fine LWA); (b) NS-SS-RLC (Coarse NWA replaced with LWA); (c) NS-FAC/SS-RLC (Partial replacement of Fine NWA with FAC and NWA Coarse replaced with LWA); and (d) NS-FAC/RLF-RLC (complete replacement of NWA with FAC, fine LWA, and coarse LWA).

lightweight phase would promote the initiation and faster propagation of stress cracks. Further discussion on the microscopic damage is provided in greater detail later in Section 3.2. The results show that, at a density around 1600–1800 kg/m^3, the compressive strength of LWC becomes insensitive to the use of steel fiber reinforcement. The elastic modulus, on the other hand, is roughly proportional to the material density regardless of the aggregates and binder type, see Fig. 6(b). The substitution of NWA by FAC and LWA leads to an elastic moduli decrease of 0.2 GPa for every 100 kg/m^3 density decrease.

3.1.2. Thermal properties

The thermal conductivity, specific heat capacity, and thermal diffusivity tested by the TPS method are summarized in Table 3, and the thermal conductivity and specific heat capacity are plotted against material density in Fig. 7. The thermal conductivity of building materials affects the heat transmission resistance of building components (i.e., R-value); while specific heat and density dictate their capabilities to store thermal energy and are important for building energy consumption and thermal comfort under transient conditions. Fig. 7(a) and (b) show the relationship between concrete density and thermal properties. Thermal conductivity of tested LWAC depends on aggregate porosity but also on their mineralogical compositions [13]. XRD analysis performed on the expanded clay LWA and FAC indicates that they both contain crystalline minerals such as quartz, calcite and mullite, see Fig. 3(a). Thus, the porosity brought by LWA and FAC makes the thermal conductivity of concrete decrease almost linearly with the decrease of material density. With respect to the decrease of the concrete density, the thermal conductivities of concretes made of normal and high strength binders decrease at a similar rate. It is noted that the thermal conductivities tested in this research are in general higher than the density based thermal conductivity equation proposed by Valore [27,28] and as shown in Fig. 7(a) where tested values are compared with the ACI 122 equation [29]. This is as expected since the lower W/C ratio used in modern concrete leads to higher thermal conductivity of the mortar matrix and the aggregates used nowadays contain large amount of quartz and other crystalline minerals that have high conductivities (4–12 W/m K [30]). Fig. 7(b) shows that the volumetric heat capacity decreases proportionally with the decrease of concrete density, i.e., the specific heat of LWC is similar to that of NWC. The thermal diffusivity, κ, is combination of thermal conductivity k and specific heat c_p: $\kappa = k/(\rho c_p)$, where ρ represents the density of the material. Thus, the thermal diffusivity variation with respect to density are similar to that of the thermal conductivity, see Table 3.

3.1.3. Effects of aggregates and binder materials

Fig. 8 shows the effect of NWA substitution by FAC, fine LWA, and coarse LWA on concrete density, mechanical and thermal properties. High strength concrete with NWA and steel fiber has higher density (7.6%) than the NWC control specimen. Replacement of NWA by LWA decreases the concrete density and influences the properties of concrete, see Fig. 8(a). The partial

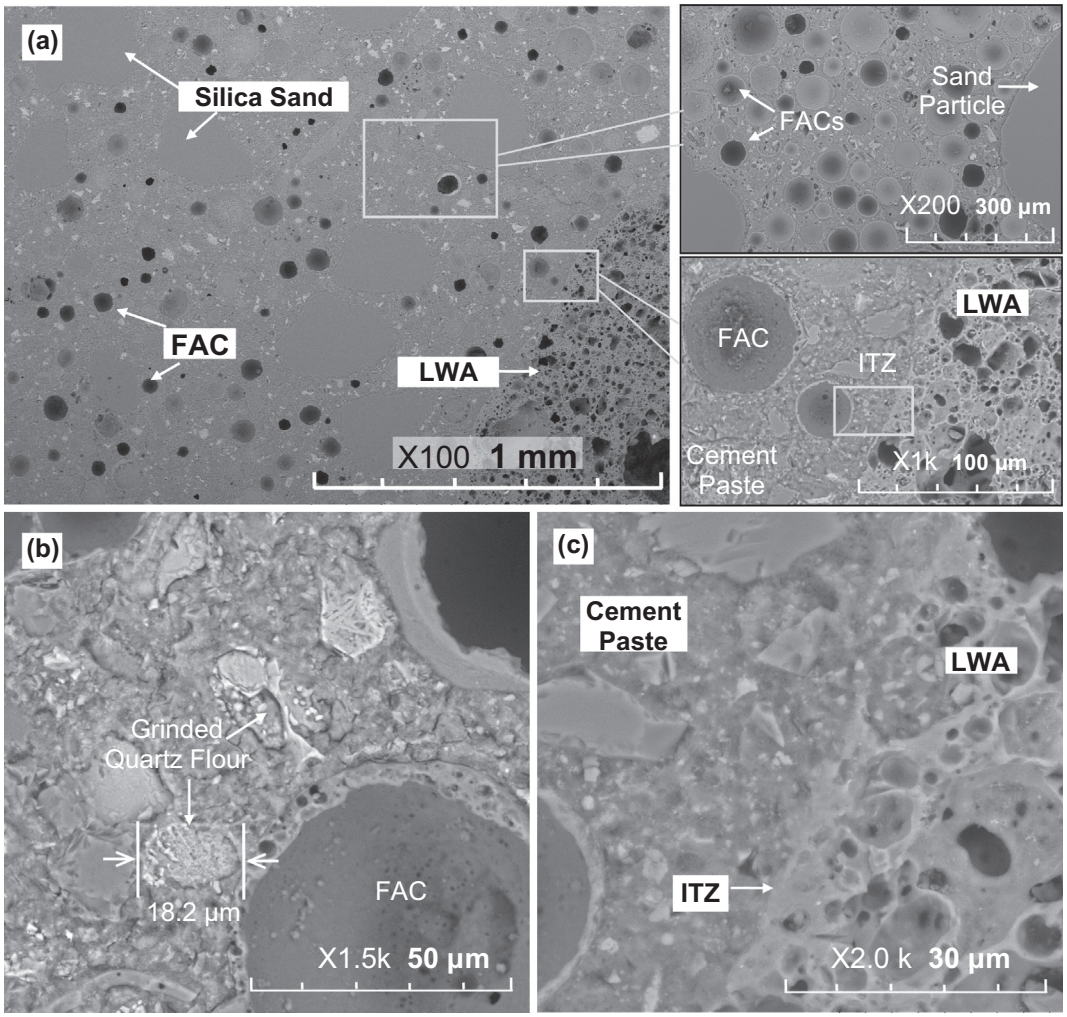

Fig. 10. SEM image showing the hierarchical microstructure the FAC-filled micro-cellular cementitious matrix and LWA.

replacement (56% by volume) of fine NWA with FAC reduces the concrete oven-dry density by approximately 6–8%; further replacement of the fine NWA by fine graded expanded clay (*RiverLite*) reduces the density by an additional 7–9%; 100% replacement of coarse NWA by LWA (*RiverLite*) reduces the concrete density by about 20%; thus, complete replacement of all NWA with FAC and LWA reduces the density by 35% (to about 1400 kg/m^3), see Table 3. The experimentally tested densities matched well with the values calculated from the mixture composition.

The substitution of coarse NWA by coarse LWA leads to 42% decrease in Young's moduli and 15–50% decrease in compressive strength depending on the binder type as shown in Fig. 8(b) and (c) respectively. Then the partial substitution of fine NWA by fly-ash cenospheres (FAC) leads to an additional decrease of 0.2–5.1 MPa and 1.3–2.5 GPa per every 100 kg/m^3 density decrease for the compressive strength and the modulus of elasticity, respectively. The compressive strength and elastic modulus decrease at faster rates when NWA are substituted with FAC and LWA for concrete having higher binder strength (i.e., cementitious matrix with silica fume and steel fiber).

Fig. 8(d) shows the effect of NWA substitution on the thermal conductivity of LWC. The thermal conductivity of LWC at 100% coarse NWA replacement decreases from 36% to 45%. The values of thermal conductivity vary from 1.0 to 1.37 W/m K. Further replacement of fine NWA with fly-ash cenospheres leads to an additional 20–25% decrease in thermal conductivity, i.e., the LWC with coarse LWA and 50% sand replaced by FAC have conductivities around 0.71–0.85 W/m K, which are about 35–40% of NWC conductivity (1.82–2.11 W/m K). The volumetric heat capacity, c_v, of concretes tested are roughly proportional to the material density, see Fig. 7(b). The specific heat, c_p, of the aggregates used in this research are in similar range – i.e., LWA, FAC, and limestone are tested at 675 J/kgK, 658 J/kgK, and 750 J/kgK, respectively under oven-dry condition.

3.2. Microstructures and damage

The microstructural characterization was carried out using both optical and scanning electron microscopic (SEM) imaging. The concrete and mortar samples for microstructural analysis were resin-impregnated using epoxy, and the resin mounted samples were then ground and polished using a *Buehler EcoMet* grinder/polisher to 0.3 µm diamond paste. Some polished samples were then carbon-coated to a thickness of approximately 10 nm to prevent charging under the electron beam. SEM imaging was conducted using a *Hitachi TM1000* at accelerating voltage of 15 kV. To analyze the fracture surfaces of the mechanically tested samples, fragments of the tested compression cylinders were preserved for SEM imaging analysis.

Fig. 9(a)–(d) present the optical microscopic images of LWC with coarse NWA and 100% substitution of fine NWA with FAC and fine-graded LWA, LWC with coarse LWA and fine NWA, LWC

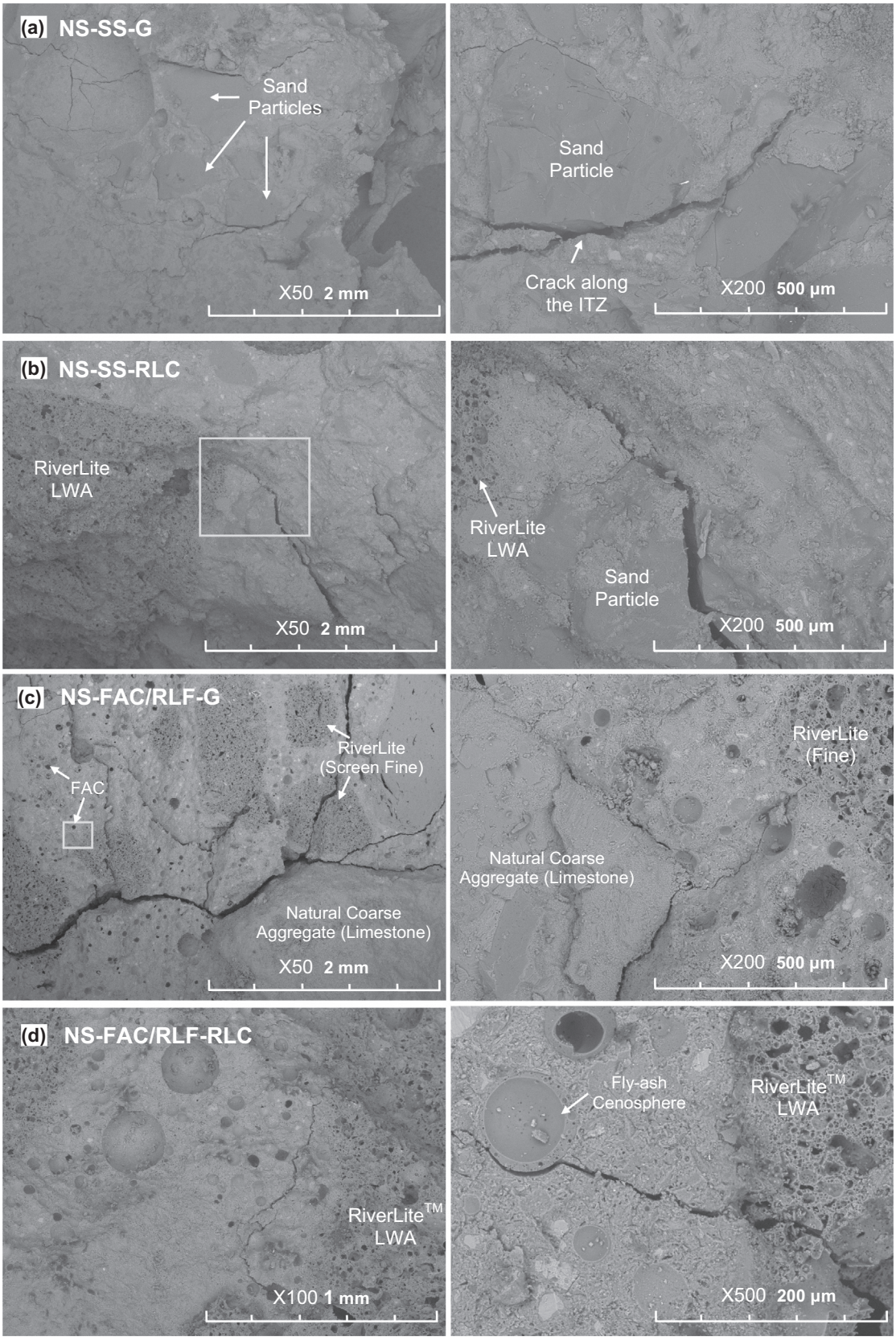

Fig. 11. Fracture topographic images of (a) NWC (reference); (b) LWC with coarse LWA; (c) LWC with fine NWA substitute by FAC and fine LWA; and (d) LWC with 100% substitution of fine and coarse NWA.

with coarse LWA and 50% substitution of fine NWA by FAC, and LWC with coarse LWA and 100% substitution of fine NWA with FAC and fine-graded LWA, respectively. The corresponding densities and compressive strengths obtained for these LWCs are 1880 kg/m^3 (51.1 MPa), 1614 kg/m^3 (39.1 MPa), 1507 kg/m^3 (39.1 MPa), 1224 kg/m^3 (33.4 MPa), respectively. The substitution

of NWA with FAC and LWA leads to lower thermal conductivities. The heat conduction in porous material results from the thermal conductivity of the solid phase of aggregate (minerals) and that of the gas or fluid phase contained in the pores. Substituting NWA in concrete by FAC and LWA leads to an increase of the voids in the concrete. Consequently, the conduction surface of the solid phase decreases whereas that of the gas phase increases. For mixes having similar density, lower thermal conductivities were tested for samples with NWA substituted by FAC and fine-graded LWA. This is consistent with the theory of Maxwell-Eucken limits [31]. For materials that are 'externally porous', where the continuous phase has lower thermal conductivity than the dispersed phase, see Fig. 9(a) and Table 2 for the thermal conductivities of each constituent phase, the heat does not have a continuous path through the more conductive phase (natural NWA); whereas an "internally porous" material consists of a continuous phase that has higher thermal conductivity than that of the dispersed phase (Fig. 9(b)). In this case, the continuous phase forms an uninterrupted pathway through the material. Holding all other variables constant, concrete that is externally porous has lower thermal conductivity than if it was internally porous [32]. Thus, inducing micro air-cells into the cement matrix via FAC leads to faster decrease in thermal conductivity than replacing coarse NWA with LWA. The lowest thermal conductivity is obtained for LWC with all NWA substituted by FAC and LWA at 0.42 W/m K, which is only about 25% of that of NWC (1.8–2.0 W/m K), see Fig. 9(d).

Fig. 10(a) shows the hierarchical microstructure of LWC with FAC-filled micro-cellular cement binder and LWA. For concrete with the high strength (HS) binder, the addition of fine-ground quartz flour and lower W/C lead to an increase in thermal conductivity. The average particle sizes of coarse aggregate, silica sand (fine NWA), fly-ash cenosphere (FAC), and quartz flour (Fig. 10(b)) are 4 mm, 0.6 mm, 81 μm, and 14 μm, respectively. The sizes of these filler/aggregate materials are distributed across a wide range along the length scales. Thus, smaller size particles within the mixture can be packed in the void volume among larger size particles. The packing of different size filler/aggregates decreases the tendency of segregation and reduces air voids, which will lead to better mechanical performance of the concrete. The polished section of LWC confirmed that all material phases are well distributed despite their large differences in density. Since most air pores in the LWA used are closed-cell pores, only a small amount of cement paste penetrated into LWA during mixing, see Fig. 10(c). This penetration of fresh cement paste into the surface pores of LWA enhances the interfacial transition zone (ITZ) and may contribute to the improvement of mechanical properties.

The fracture surfaces of the compressive cylinders used for the mechanical testing were also examined using SEM. Fig. 11(a)–(d)

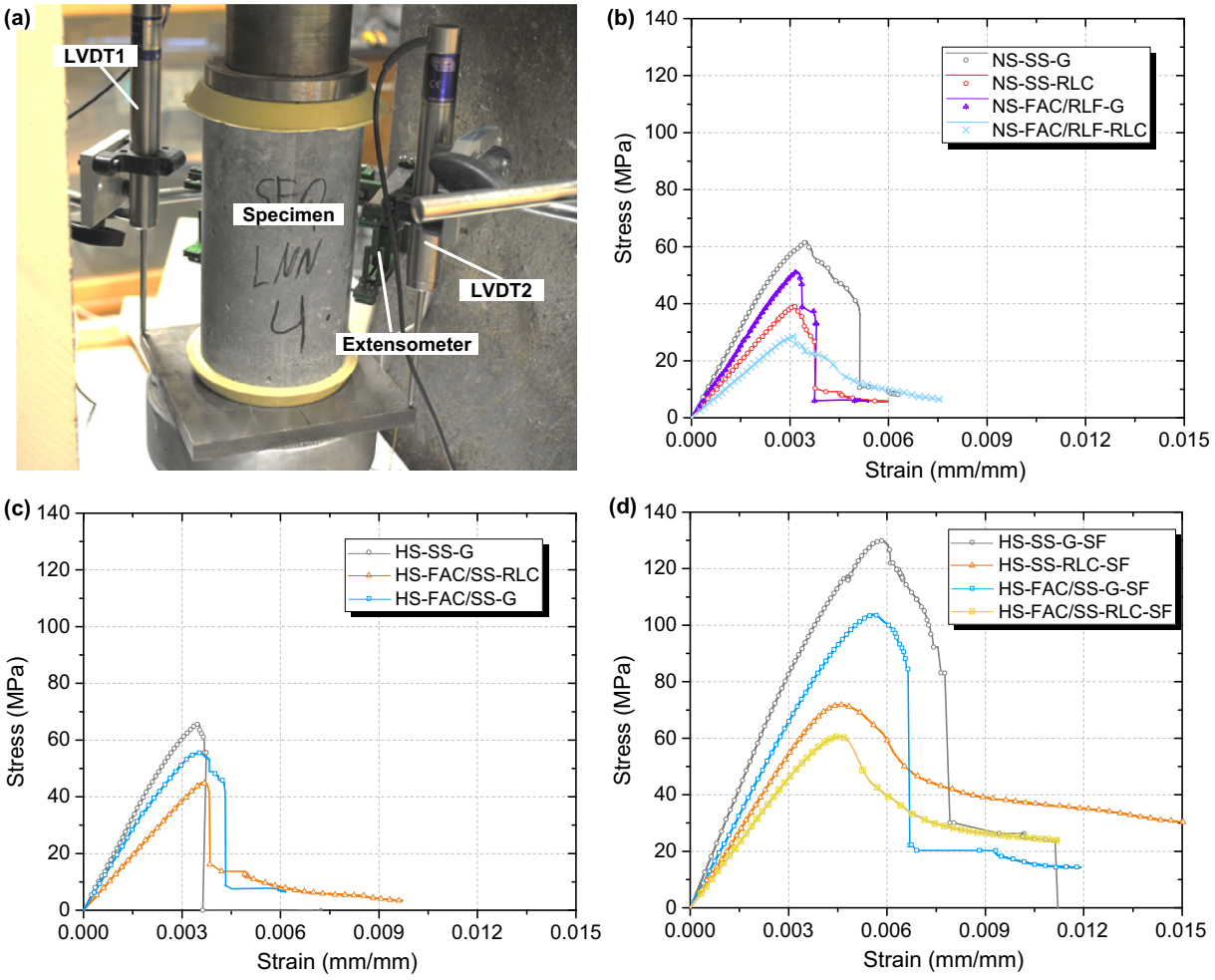

Fig. 12. Stress–strain behavior: (a) experimental test setup; representative stress–strain curves of (b) concrete with normal strength binder; (c) concrete with high strength binder (low w/c + silica fume + quartz powder filler); and (d) concrete with high strength binder reinforced with steel fiber.

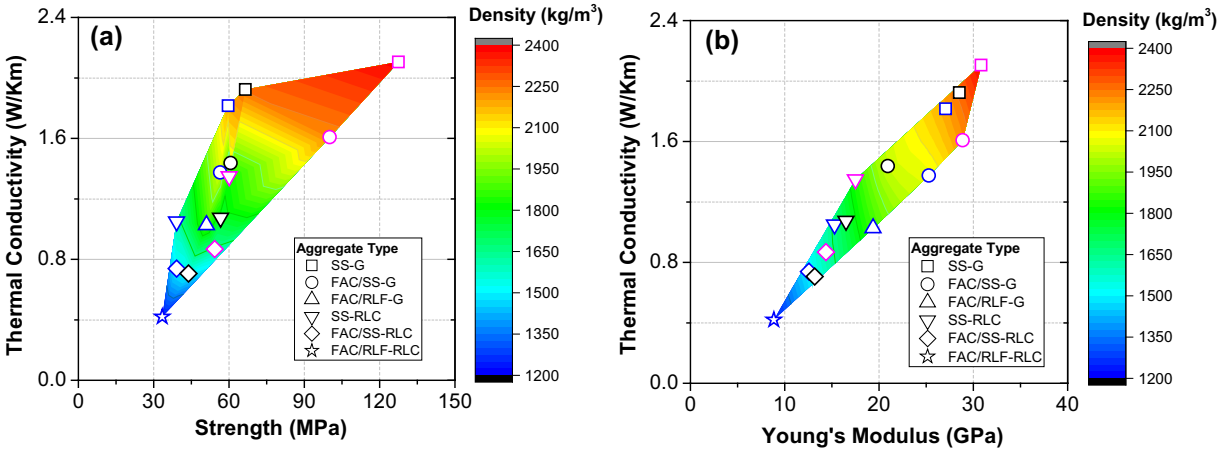

Fig. 13. Relationship between (a) thermal conductivity vs. compressive strength; and (b) thermal conductivity vs. elastic modulus.

present the fracture topographical images of NWC, LWC with coarse NWA substituted by coarse LWA, LWC with fine NWA substitute by FAC and fine LWA, and LWC with 100% substitution of fine and coarse NWA, respectively, all containing NS binder. It is evident that the damage modes of materials at microscopic scale are different for LWC with the various aggregate/filler types. For NWC containing only NWA, stress cracks tend to initiate and develop within and along the interfacial transition zone (ITZ). While the fracture of coarse NWA (limestone gravel) were observed for NWC, cracks normally propagate along the ITZ between fine NWA and the cement paste, see Fig. 11(a). For LWCs containing LWA, stress cracks normally propagate through the porous LWA, see Fig. 11(b) and (c). Whereas for LWC with FAC and fine LWA, the stress cracks normally propagate through fine LWA and along the ITZ between coarse NWA and the matrix, see Fig. 11(c). Examination of the fracture surface indicates that many coarse NWA in this type of LWC exhibit 'pull-out' failure. As a result, for concrete with similar density, the materials with fine NWA substituted by FAC and fine graded LWA exhibit more ductile behavior than the ones having coarse LWA. Fig. 12 presents the stress–strain curves obtained for representative samples within each material group, where Fig. 12(a) shows the test setup and Fig. 12(b)–(d) show the stress–strain curves for concretes with normal strength binder (NS-xxx-xxx), high strength (HS-xxx-xxx), and steel fiber reinforced high strength binder (HS-xxx-xxx-SF), respectively. In addition, LWC containing fly ash cenospheres (FAC) generally exhibit good mechanical performance. Owing to the partial pozzolanic reactivity and micro-porous surface, the FAC particles bonded well with the cementitious matrix [33]. The relatively small particle size and strong shell of E106 FAC allows the FAC to act as barriers to hinder the propagation of stress cracks, see Fig. 11(d).

3.3. Balancing mechanical and thermal properties of LWCs

Fig. 13(a) and (b) show the relationship between the compressive strength and the thermal conductivity of the various types of concrete investigated in this research. The color contour indicates oven-dry density of the materials. It is noted that all concrete mixtures studied in this research have compressive strength greater than 30 MPa and have sufficient strength to be used for structural purposes. When the thermal conductivity is less than 0.8 W/m K, LWC with different binder materials (i.e., normal strength or high strength binders) have similar compressive strength (Fig. 12(a)). On the contrary, when thermal conductivity is higher than 0.8 W/m K (density greater than 1400 kg/m^3), LWC with steel fiber reinforced high strength cementitious matrix gives the highest compressive strength. The LWC with fiber reinforced high strength binder have the best strength/conductivity ratio. Young's moduli are almost linearly correlated to thermal conductivities regardless the binder materials and aggregate type. For the concrete tested in this study, the dry density needs to be greater than 1800 kg/m^3 for the Young's modulus to be greater than 18 GPa. The lightest concrete (1220 kg/m^3) with 100% NWA substitution has moderate strength (33.4 MPa) and low elastic modulus (8.8 GPa), which may be suitable for the use in non-critical structural components such as roof slab and infill wall panels.

4. Thermal properties of lightweight concrete containing FAC and aggregates

4.1. A two-step homogenization scheme

In a composite material system, inclusions of different sizes will be categorized as belonging to a different scale if the properties of larger sized inclusions are not affected by each individual smaller size inclusion. In that case, the larger inclusions see the original matrix materials and the smaller inclusions as new homogenous matrix [34]. Thus, the determination of effective (homogenized) thermal property of lightweight concrete and cementitious composites containing lightweight aggregates (LWAs) and fly-ash cenospheres (FAC) can be calculated using a two-step homogenization scheme as shown in Fig. 14. First, the effective thermal property of cement paste containing polydispersed FACs is calculated as a composite system containing core-shell inclusions [14]. To calculate the effective thermal conductivity (ETC) of this microstructure, Felske's equations are used where the ETC of cement paste containing FACs is calculated as a function of the properties of each composing phase (i.e., cement paste matrix, FAC shell, and air enclosed in FAC particles, see Fig. 14(a)) and their relative volume fractions. Then, the ETC of lightweight concrete containing aggregates can be calculated using two-phase homogenizations models (Fig. 14(b) and (c)). All thermal properties for the constituent phases used in this research are listed in Table 2.

4.2. Effective thermal properties of lightweight concrete containing FAC

In a previous work by the authors [14], we demonstrated that the effective thermal conductivity (ETC) of cement mortars containing polydispersed core-shell particles can be estimated using Felske's equation [35]. For fly-ash cenospheres (FAC) that have

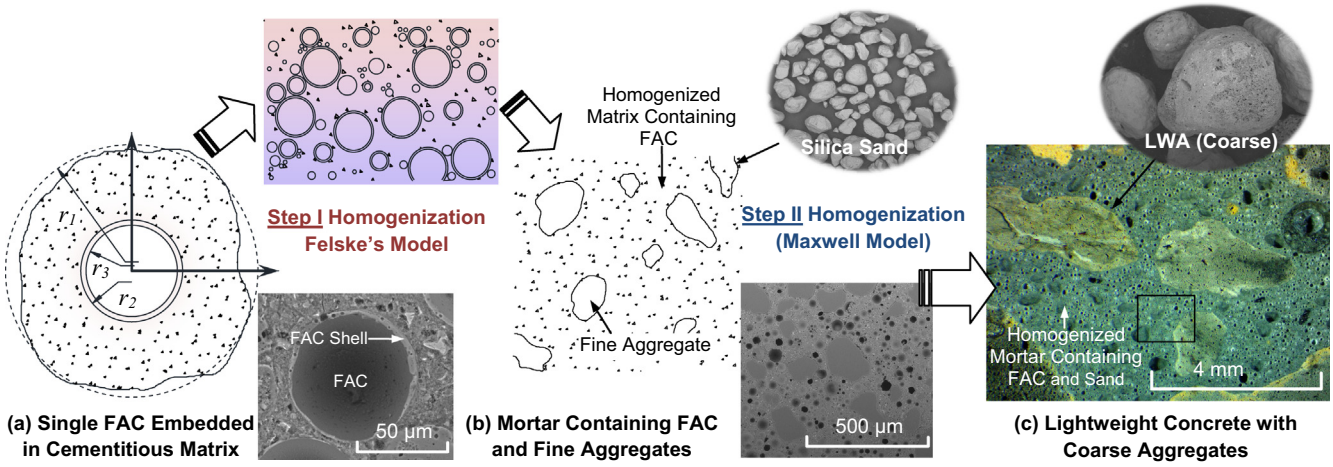

Fig. 14. Microstructure and effective thermal conductivity of lightweight cementitious composite (LWCC): (a) a RVE containing one single microsphere particle; (b) mortar with polydispersed microsphere particles and fine aggregates; and (c) LWC with coarse aggregates.

perfect thermal conduct with the cementitious matrix, the ETC can be expressed in a simple form as:

$$k_{eff} = \left(\frac{1 + 2\Theta v_f}{1 - \Theta v_f}\right) k_1 \tag{3}$$

where

$$\Theta = (\eta - 1)/(\eta + 2) \tag{4}$$

and

$$\eta = 2k_{21}u/(3\rho_s - u) \tag{5}$$

where $k_{21} = k_2/k_1$, k_1 and k_2 denote the thermal conductivities of the cement paste and FAC shell, respectively; and u is the nominal density of FAC which can be measured experimentally using gas pycnometry [36]. Thus, the ETC of cement paste filled with FACs can be simply expressed in terms of the FAC volume fraction v_f, the thermal conductivities of cement paste, k_1, the FAC shell, k_2, and the measured density of FAC particles, u. It is noted that Eqs. ((3)–(5)) circumvent the tedious experimental determination (even if possible) of thermal conductivity of polydispersed hollow FACs, and use only particle density and shell properties (i.e., both can be easily measured experimentally –) to obtained the ETC of the composite system. The effective volumetric heat capacity of cement paste containing FACs can be expressed as (the heat capacity of air is neglected):

$$(\rho c_p)_{eff} = \frac{1}{V}\frac{\partial \sum H}{\partial T} = (1 - v_f)(\rho c_p)_1 + \left(1 - \frac{1}{v_{f3}}\right) v_f (\rho c_p)_2 \tag{6}$$

where T is temperature; ρ is density; H is enthalpy; and c_p is specific heat capacity of the solid material phases; $v_{f3} = v_f/v_3$ and v_3 is the volume fraction of the air core within FAC. For the hollow FAC, v_{f3} can be rewritten as a function of the shell density, ρ_s, and particle density, u, as $v_{f3} = \rho_s/(\rho_s - u)$.

Once the homogenized thermal properties of cement paste containing FACs are obtained, the ETC of mortar and concrete containing aggregates can be obtained by treating FAC filled

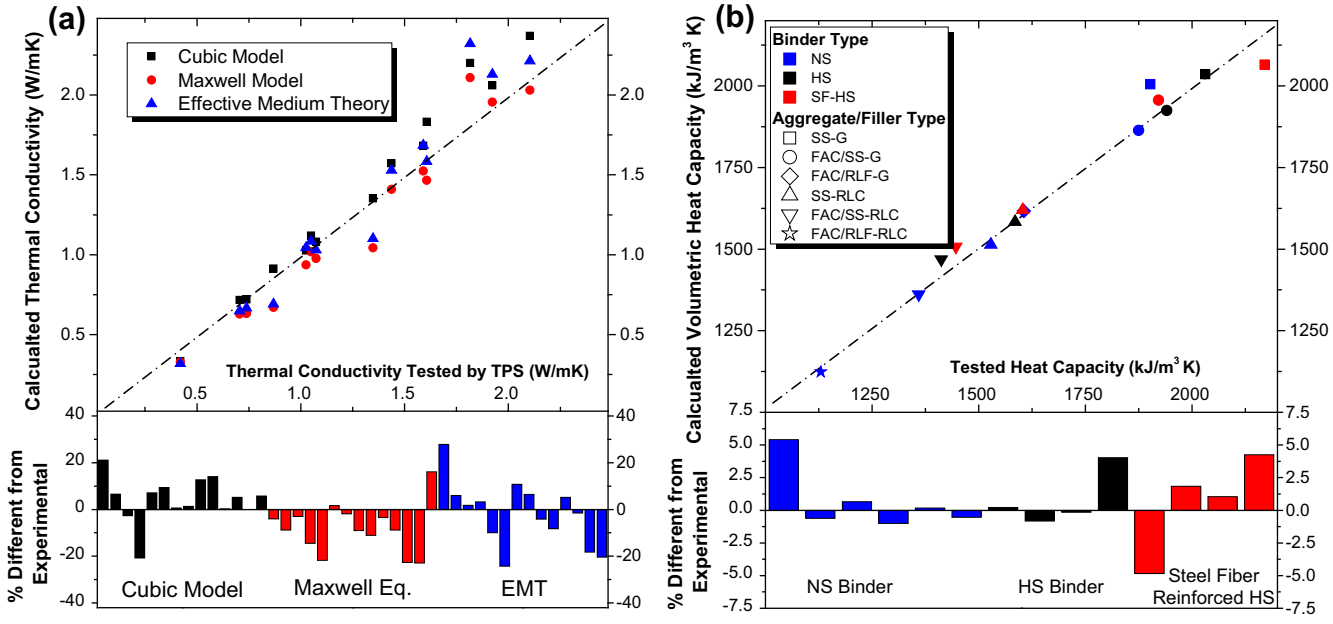

Fig. 15. Comparison between calculated and experimental results: (a) thermal conductivity; and (b) volumetric heat capacity.

cement paste as a homogenized matrix, see Fig. 14(b). For aggregates of different length scales (i.e., fine-ground mineral powder, sand, and course aggregates), the homogenization model can be repeated. In this paper, three popular two-phase homogenization models – including the parallel and series models (e.g., the cubic model proposed by Valore and Green [37]), Maxwell model [31], and the effective medium theories (EMT) [38] were used to calculate the ETC of lightweight concretes containing fine and coarse aggregates. The results are compared in Fig. 15 together with the experimental data. For all 14 concrete mixtures tested in this study, the calculated ETCs coincide well with the experimental results – i.e., the differences are generally within 20% (Fig. 15(a)). Fig. 15(b) presents the calculated volumetric heat capacities of concrete in comparison with the experimentally tested values. Good agreement was found between the experimental data and calculated results. Some sources for discrepancy may include the deviation of actual volume fractions of each constituents from the design values (i.e., which may be a results of the variation of water content of aggregates for each batch), the variations of the aggregate distribution between each tested specimen, experimental errors, etc.

5. Conclusions

A study was conducted on lightweight concrete (LWC) containing various types of aggregates – i.e., lightweight aggregates (LWA), nature normal weight aggregates (NWA) – and fly-ash cenospheres (FAC) lightweight functional filler to evaluate the influence of aggregate properties and their volume fractions on both the mechanical and thermophysical properties of LWC. The microstructures of LWC were analyzed for both pristine and mechanically tested samples. Key parameters governing thermal and mechanical properties of the LWC are discussed and the composition-property relationships are deduced from both experimental results and predictive models. The following conclusions are drawn from this study:

- The thermal properties (i.e., thermal conductivity and specific heat capacity) of LWC are primarily dictated by the volume fraction of LWA and concrete density. On the other hand, the compressive strength of LWC is affected by the size and properties of the LWA used in the mixture – i.e., smaller size LWA had less adverse impact on concrete strength. In addition, replacing normal weight aggregates (NWA) in higher strength mixtures with LWA would result in faster strength declination. The Young's moduli of LWCs are found to be roughly proportional to concrete dry density.
- Incorporating micro-size fly ash cenospheres (FAC) into the cementitious matrix can effectively reduce the density and thermal conductivity of concrete by inducing a micro-cellular structure to the matrix phase. The strong shell and small particle size of FAC may provide barriers to hinder crack propagation. SEM analysis performed on the mechanically tested LWC samples revealed that some FACs with smaller particle size and thicker shell walls would survive the mechanical loading and show "pull-out" failure. In addition, introducing small and spherical FAC particles may also improve the rheological properties of concrete by allowing the FAC to roll among angular aggregates during mixing.
- The two-step homogenization scheme proposed in this study can predict the thermal properties of lightweight concrete with good accuracy, where the Felske equation provides a simple yet accurate method to calculate the thermal property of cement mortar containing FAC and the effects of fine and coarse aggregates can be estimated using two-phase homogenization models.
- Lastly, by carefully selecting the mixture design and constituent materials (e.g., types of aggregates and lightweight functional fillers), LWC with high strength and low thermal conductivity can be developed for the use in energy-saving building design.

Conflict of interest

None.

Acknowledgements

This research is partially sponsored by US National Science Foundation (CMMI-1663302) and the University of Alabama in Huntsville (UAH) through faculty startup funding. The funding supports from NSF and UAH are greatly appreciated. The authors would like to thank Mr. Dominic Hanna for his assistance during the experimental phase. The authors would also like to thank Trinity Lightweight (Mr. Jeffery Speck) for donating the lightweight aggregates used for the experiments and Dr. Wei Tian from Chang'an University for running the MIP analysis.

References

[1] S. Chandra, L. Berntsson, Lightweight Aggregate Concrete: Science, Technology, and Applications, Noyes Publications, New York, 2002.
[2] D. Kramar, V. Bindiganavile, Mechanical properties and size effects in lightweight mortars containing expanded perlite aggregate, Mater. Struct. 44 (2011) 735–748, https://doi.org/10.1617/s11527-010-9662-0.
[3] M. Lanzón, P.A. García-Ruiz, Lightweight cement mortars: advantages and inconveniences of expanded perlite and its influence on fresh and hardened state and durability, Constr. Build. Mater. 22 (2008) 1798–1806, https://doi.org/10.1016/j.conbuildmat.2007.05.006.
[4] Z. Lu, B. Xu, J. Zhang, Y. Zhu, G. Sun, Z. Li, Preparation and characterization of expanded perlite/paraffin composite as form-stable phase change material, Solar Energy 108 (2014) 460–466, https://doi.org/10.1016/j.solener.2014.08.008.
[5] R. de Gennaro, A. Langella, M. D'Amore, M. Dondi, A. Colella, P. Cappelletti, et al., Use of zeolite-rich rocks and waste materials for the production of structural lightweight concretes, Appl. Clay Sci. 41 (2008) 61–72, https://doi.org/10.1016/j.clay.2007.09.008.
[6] Y. Ke, A.L. Beaucour, S. Ortola, H. Dumontet, R. Cabrillac, Influence of volume fraction and characteristics of lightweight aggregates on the mechanical properties of concrete, Constr. Build. Mater. 23 (2009) 2821–2828, https://doi.org/10.1016/j.conbuildmat.2009.02.038.
[7] A. Lotfy, K.M.A. Hossain, M. Lachemi, Lightweight self-consolidating concrete with expanded shale aggregates: modelling and optimization, Int. J. Concr. Struct. Mater. 9 (2015) 185–206, https://doi.org/10.1007/s40069-015-0096-5.
[8] J.L. Clarke (Ed.), Structural Lightweight Aggregate Concrete, Blackie Academic & Professional, London and New York, 1993.
[9] ACI Committee 213. Guide for Structural Lightweight-Aggregate Concrete. 2014.
[10] American Society for Testing and Materials. Standard Specification for Lightweight Aggregates for Structural Concrete. 2017. doi: 10.1520/C0330.
[11] America Concrete Institute. Standard Practice for Selecting Proportions for Structural Lightweight Concrete (ACI 211 . 2–98). 1998.
[12] M. Hassanpour, P. Shafigh, H. Bin, Lightweight aggregate concrete fiber reinforcement – A review, Construct. Build. Mater. 37 (2012) 452–461, https://doi.org/10.1016/j.conbuildmat.2012.07.071.
[13] L.H. Nguyen, A.L. Beaucour, S. Ortola, A. Noumowé, Influence of the volume fraction and the nature of fine lightweight aggregates on the thermal and mechanical properties of structural concrete, Constr. Build. Mater. 51 (2014) 121–132, https://doi.org/10.1016/j.conbuildmat.2013.11.019.
[14] A.L. Brooks, H. Zhou, D. Hanna, Comparative study of the mechanical and thermal properties of lightweight cementitious composites, Constr. Build. Mater. 159 (2018) 316–328, https://doi.org/10.1016/j.conbuildmat.2017.10.102.
[15] Y. Wu, J.Y. Wang, P.J.M. Monteiro, M.H. Zhang, Development of ultra-lightweight cement composites with low thermal conductivity and high specific strength for energy efficient buildings, Constr. Build. Mater. 87 (2015) 100–112, https://doi.org/10.1016/j.conbuildmat.2015.04.004.
[16] B. Xu, H. Ma, C. Hu, S. Yang, Z. Li, Influence of curing regimes on mechanical properties of magnesium oxychloride cement-based composites, Constr. Build. Mater. 102 (2016) 613–619, https://doi.org/10.1016/j.conbuildmat.2015.10.205.
[17] F. Liu, J. Wang, X. Qian, J. Hollingsworth, Internal curing of high performance concrete using cenospheres, Cem. Concr. Res. 95 (2017) 39–46, https://doi.org/10.1016/j.cemconres.2017.02.023.

[18] K.V. Joseph, F. Francis, J. Chacko, P. Das, G. Hebbar, FLY ash cenosphere waste formation in coal fired power plants and its applications a structural material-a review, Int. J. Eng. Res. Technol. 2 (2013) 18–21.
[19] X. Huang, R. Ranade, Q. Zhang, W. Ni, V.C. Li, Mechanical and thermal properties of green lightweight engineered cementitious composites, Constr. Build. Mater. 48 (2013) 954–960, https://doi.org/10.1016/j.conbuildmat.2013.07.104.
[20] Q.L. Yu, P. Spiesz, H.J.H. Brouwers, Ultra-lightweight concrete: conceptual design and performance evaluation, Cem. Concr. Compos. 61 (2015) 18–28, https://doi.org/10.1016/j.cemconcomp.2015.04.012.
[21] A.A. Sayadi, J.V. Tapia, T.R. Neitzert, G.C. Clifton, Effects of expanded polystyrene (EPS) particles on fire resistance, thermal conductivity and compressive strength of foamed concrete, Constr. Build. Mater. 112 (2016) 716–724, https://doi.org/10.1016/j.conbuildmat.2016.02.218.
[22] S.E. Gustafsson, Transient diffusivity plane source techniques for thermal conductivity measurements of solid materials and thermal, Rev. Sci. Instrum. 62 (1991) 797–804.
[23] Y. He, Rapid thermal conductivity measurement with a hot disk sensor: Part 1 Theoretical considerations, Thermochim. Acta 436 (2005) 122–129, https://doi.org/10.1016/j.tca.2005.06.026.
[24] A. Berge, B. Adl-Zarrabi, C.E. Hagentoft, Determination of specific heat capacity by transient plane source, Front. Arch. Res. 2 (2013) 476–482, https://doi.org/10.1016/j.foar.2013.09.004.
[25] ISO22007-2:2008. Plastics – Determination of thermal conductivity and thermal diffusivity – Part 2: Transient plane source method. 2008.
[26] H. Yan, W. Sun, H. Chen, Effect of silica fume and steel fiber on the dynamic mechanical performance of high-strength concrete, Cem. Concr. Res. 29 (1999) 423–426, https://doi.org/10.1016/S0008-8846(98)00235-X.
[27] R.C.J. Valore, Calculation of U-Values of hollow concrete masonry, Concr. Int. Am. Concr. Inst. 2 (1980) 40–63.
[28] R.C. Valore, The Thermophysical Properties of Masonry and Its Constituents, International Masonry Institute, Washington, DC, 1988.
[29] ACI Committee 122. Guide to Thermal Properties of Concrete and Masonry Systems. 2002.
[30] C. Clauser, E. Huenges. Thermal Conductivity of Rocks and Minerals. In: Ahrens TJ, editor. Rock Phys. Phase Relations A Handb. Phys. Constants. Therm. Conduct. Rocks Miner., 1995, p. 105–26. doi: 10.1029/RF003
[31] K. Pietrak, T.S. Wisniewski, A review of models for effective thermal conductivity of composite materials, J. Power Technol. 95 (2015) 14–24.
[32] D.P. Hochstein, Thermal Conductivity of Fiber-Reinforced Lightweight Cement Composites, Columbia University, 2013.
[33] V. Rheinheimer, Y. Wu, T. Wu, K. Celik, J. Wang, L. De Lorenzis, et al., Multi-scale study of high-strength low-thermal-conductivity cement composites containing cenospheres, Cem. Concr. Compos. 80 (2017) 91–103, https://doi.org/10.1016/j.cemconcomp.2017.03.002.
[34] T. Wu, I. Temizer, P. Wriggers, Computational thermal homogenization of concrete, Cem. Concr. Compos. 35 (2013) 59–70, https://doi.org/10.1016/j.cemconcomp.2012.08.026.
[35] J.D. Felske, Effective thermal conductivity of composite spheres in a continuous medium with contact resistance, Int. J. Heat Mass Transf. 47 (2004) 3453–3461, https://doi.org/10.1016/j.ijheatmasstransfer.2004.01.013.
[36] C.L. Bielders, L.W. De Backer, B. Delvaux, Particle density of volcanic soils as measured with a gas pycnometer, Soil Sci. Soc. Am. J. 54 (1990) 822, https://doi.org/10.2136/sssaj1990.03615995005400030034x.
[37] R.C. Valore, W.C. Green, Air replaces sand in "no-fines" concrete, ACI Mater. J. 47 (1951) 833–845.
[38] T.C. Choy, Effective Medium Theory: Principles and Applications Monographs on Physics, Oxford University Press, 1999.